Thermal visualization of a heating flat surface under low frequency ultrasonic waves using liquid crystals

Author(s):
Inworn, N.; Chaiworapuek, W.

Publication date:
2018-10-05

Permanent link:
https://doi.org/10.3929/ethz-b-000279145

THERMAL VISUALIZATION OF A HEATING FLAT SURFACE UNDER LOW FREQUENCY ULTRASONIC WAVES USING LIQUID CRYSTALS

N. Inworn, W. Chaiworapuek [c]

Department of Mechanical Engineering, Faculty of Engineering, Kasetsart University, Bangkok 10900, Thailand

[c]Corresponding author: Tel.: +66-2-797-0999#1868; Fax: +66-2-579-4576; Email: fengwcc@ku.ac.th

KEYWORDS:
Main subjects: ultrasound, heat transfer, flat plate, laminar flow, liquid crystals

ABSTRACT: *Following the development of piezo-electric material, the low frequency ultrasonic waves have been found to provide a great increase in heat transfer while relatively low pressure loss occurs in the system. Hence, this paper presents the thermal visualization of a heating flat surface under the low frequency ultrasonic waves using thermochromic liquid crystals. The experiment was carried out in a water tunnel, having the flow velocities of 0.12, 0.14, and 0.17 m/s, covering the Reynolds number between 80,000 and 190,000. The 60 W ultrasonic waves, having a frequency of 25, 33, and 40 kHz were emitted from a flat ultrasonic transducer in downward direction, perpendicular to the mainstream flow. The flat surface, having a constant heat flux of 1,875 W/m2 was coated with liquid crystals to reveal the heat transfer mechanism qualitatively and quantitatively. The results showed that the region of enhanced heat transfer occurred like wedge structure, caused by the bubbles from acoustic cavitation phenomenon. This region moved further downstream following the increase in Reynolds number. The magnitude of the Nusselt number and size of the distribution enlarged proportionally with the wave frequency. At the relatively low Reynolds number, the maximum Nusselt number is up to 14%, 17.5%, and 21.8%, at the wave frequency of 25, 33, and 40 kHz, respectively. These obtained information clarified the process of heat transfer enhancement using the low frequency ultrasonic waves.*

1 Introduction

The ultrasonic waves are the acoustic wave, having the frequency above the human hearing range or about 20 kHz. Recently, interest in the use of ultrasonic waves, especially in heat transfer application has grown following the technological advancement of piezo-electric materials. They can be categorized as 3 types following their frequency, f. The waves are called "low frequency ultrasonic waves" or "power ultrasonic waves" when the wave frequency is between 20 – 100 kHz. If f is between 100 – 1,000 kHz, the ultrasound is defined as high frequency ultrasound [1]. Above these ranges, they are referred to very high frequency ultrasonic waves. When these waves propagate in the liquid medium, two important phenomena, relating to the heat transfer enhancement includes acoustic cavitation and acoustic streaming. The acoustic cavitation occurs when the pressure of liquid medium decreases during the rarefaction range of the waves [2]. The bubbles are rapidly formed, expanded, and then exploded violently [3]. This effect usually appears under the low frequency ultrasound. In the meantime, the acoustic streaming is a time-averaged streaming, driven in a fluid flow domain by the wave power [4]. It is induced by the dissipation of acoustic energy flux, causing the momentum flux gradients to generate the acoustic streaming flow. The occurrence of these effects permits the destabilization of boundary layer, leading to the augmentation of heat transfer.

The technique of heat transfer enhancement using the ultrasonic waves was first investigated by [5]. They visualized the thermoacoustic streaming around a heating cylinder using smoke. Their results revealed that the streaming, appearing as vortices, begins when the sound level reaches a critical sound pressure level. At a higher sound pressure level, the vortex streaming becomes fully developed. However, when the ultrasound is applied to the liquid, not only acoustic streaming but also other effects such as the acoustic cavitation, vibration, and fouling reduction, etc. emerge simultaneously in a fluid domain [1]. These effects strongly depend on the power and frequency of the ultrasonic waves. The wave power has been found to boost the wave intensity that is able to disturb the velocity and thermal boundary layers. With a 50% increase of the wave power, the factor of heat transfer enhancement gains up to 27% [6-8]. The wave frequency is also a main factor, having a great impact on the heat transfer. On a flat plate, the Nusselt number can be increased approximately 11% when the wave frequency is changed from 25 to 40 kHz [9]. Under these wave frequencies, the acoustic streaming of low frequency ultrasound is strengthened when the bubbles occur [10]. Besides, the beam direction of the streaming can be altered by the change of mainstream velocity [11]. Therefore, the inclination of the beam, occurring with the variation of mainstream velocity, must be considered in order to use the ultrasound to enhance the heat transfer.

To acquire more information from this complicating mechanism of heat transfer process over a heating plate, the thermochromic liquid crystals were utilized to obtain the thermal characteristics under the 25, 33, and 40 kHz acoustic waves. The instantaneous temperature and Nusselt number contours were extracted qualitatively and quantitatively with the aid of image processing technique. Finally, the ratio Nusselt number distribution, calculated from the condition with and without ultrasound was presented and discussed. These provide useful information for numerical modelling of the heat transfer enhancement using the ultrasonic waves.

2 Experimental Setup

The experiment was conducted in a test section of a low freestream water tunnel, as depicted in Fig. 1. The test section was made from a 10 mm Perspex plate and had a size of 150 cm length * 20 cm width * 15 cm height. A bleeding channel was installed at the upstream of the test plate to refresh a new boundary layer. The test surface was prepared by covering a black 0.12 mm PVC sheet over a 3 mm thick aluminum plate. A 300 W plate heater with a length of 0.8 m was mounted underneath the test plate to create a constant heat flux condition from x = 0.3 m – 1.1 m. Between them, a 10 mm aluminum plate was inserted for a better distribution of heat transfer from the heater. A high thermal resistance insulator was laid under the heater to prevent the heat loss in a downward direction.

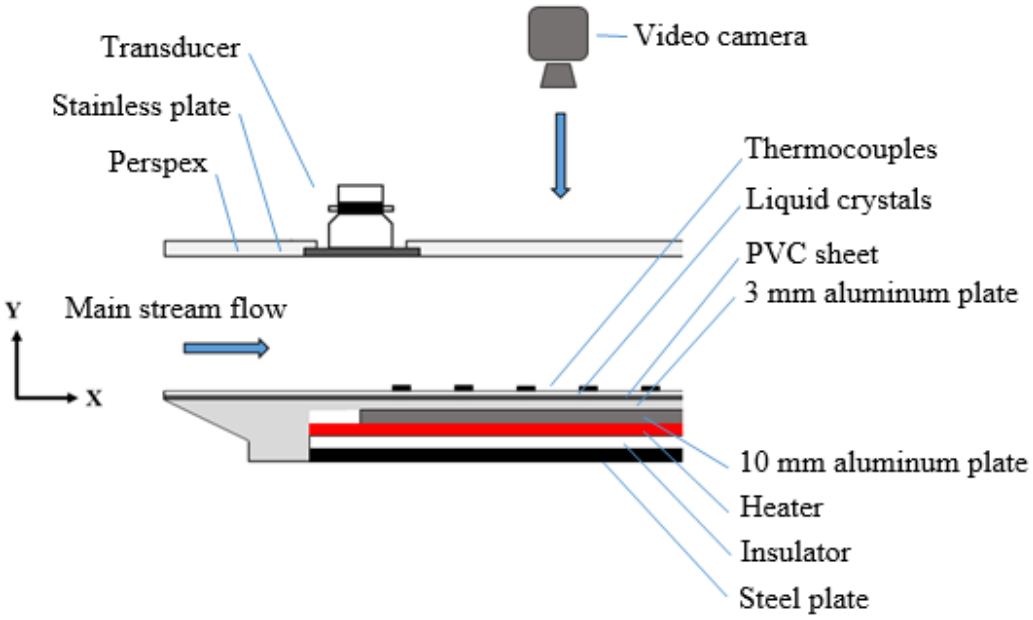

Fig. 1. Schematic view of the test section

The thermochromic liquid crystals were coated over the PVC sheet to yield the thermal information of the heating plate. The white light, containing the full spectrum of wavelengths, was illuminated with 70 W fluorescent bulbs to scatter the color of the liquid crystals. Beside the test section, a glossy reflector was attached to the light source to intense the light intensity. The active range of the liquid crystals was calibrated with the temperature, measured from thin leaf thermocouples. They were well attached on the test surface at a x = 0.47 m – 1.07 m with an increment of 0.1 m and had an uncertainty of 0.75%. The mainstream velocity was measured with a turbine flow meter, having an uncertainty of 0.35%. On the upper wall of the test section, a flat ultrasonic transducer were mounted on a 1.5 mm stainless plate, tightened with an acrylic roof as depicted in Fig. 2. The transducer was also connected with the ultrasonic generator that was able to generate ultrasonic frequencies between 20 – 40 kHz. The acoustic waves propagate from the transducer in a downward direction to induce more heat transfer rate from the heating plate. A video camera was held at a height of 1.5 m from the test surface to acquire the image of the test area, having a size of 0.45 m * 0.55 m with a resolution of 576 pixels * 704 pixels and a frame rate of 25 fps.

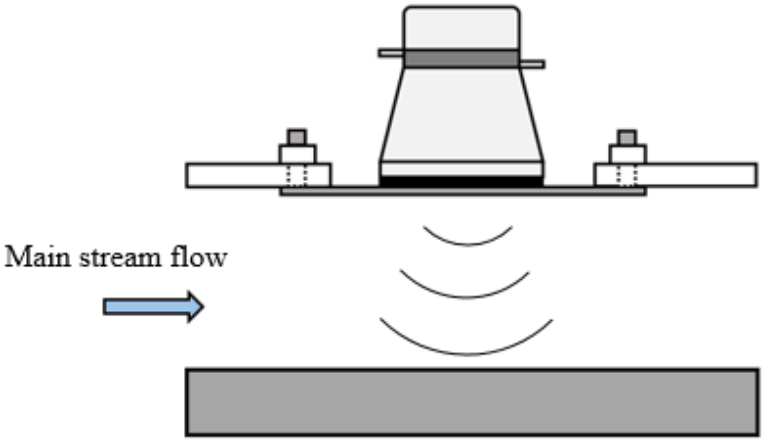

Fig. 2. Installation of the ultrasonic transducer

In the present study, the effects of wave frequencies = 25, 33, and 40 kHz on the heat transfer capability of the flat plate were investigated under the free stream velocity of U_α = 0.126, 0.141, and 0.171 m/s, called case 1, 2, and 3, respectively. The location of the ultrasonic transducer was fixed at x = 0.47 m from the plate leading edge, corresponding to the Re_x of 66,661, 74,375, and 80,776 following the mainstream velocities. At these Reynolds number, the turbulent intensity was detected below 2% and the velocity under the shear layer as depicted in Fig. 3 was captured using a Dantec fiber film probe type 55R15 with a frequency response of 30 kHz. The position of the sensor was changeable by an Arcus stepper motor model DMX-K-SA-23, having a tolerance in translation of 10 µm. The measured profile is in agreement with the Blasius profile and provides a boundary layer thickness (δ) and a boundary layer displacement thickness (δ*), as shown in Table 1. Using the δ*, the streamwise and spanwise distances are normalized as follows:

$$X = x / \delta^* \tag{1}$$

$$Y = y / \delta^* \tag{2}$$

Table 1 The local Reynolds numbers ($Re_{x,UT}$), turbulent intensity (Tu), boundary layer thicknesses (δ), and displacement thicknesses (δ*) at the position of transducer.

Case	U_α(m/s)	Tu (%)	$Re_{x,UT}$	δ (mm)	δ* (mm)
1	0.126	1.78	66,661	9.10	2.48
2	0.141	1.77	74,375	8.62	2.37
3	0.171	1.55	89,776	7.84	2.18

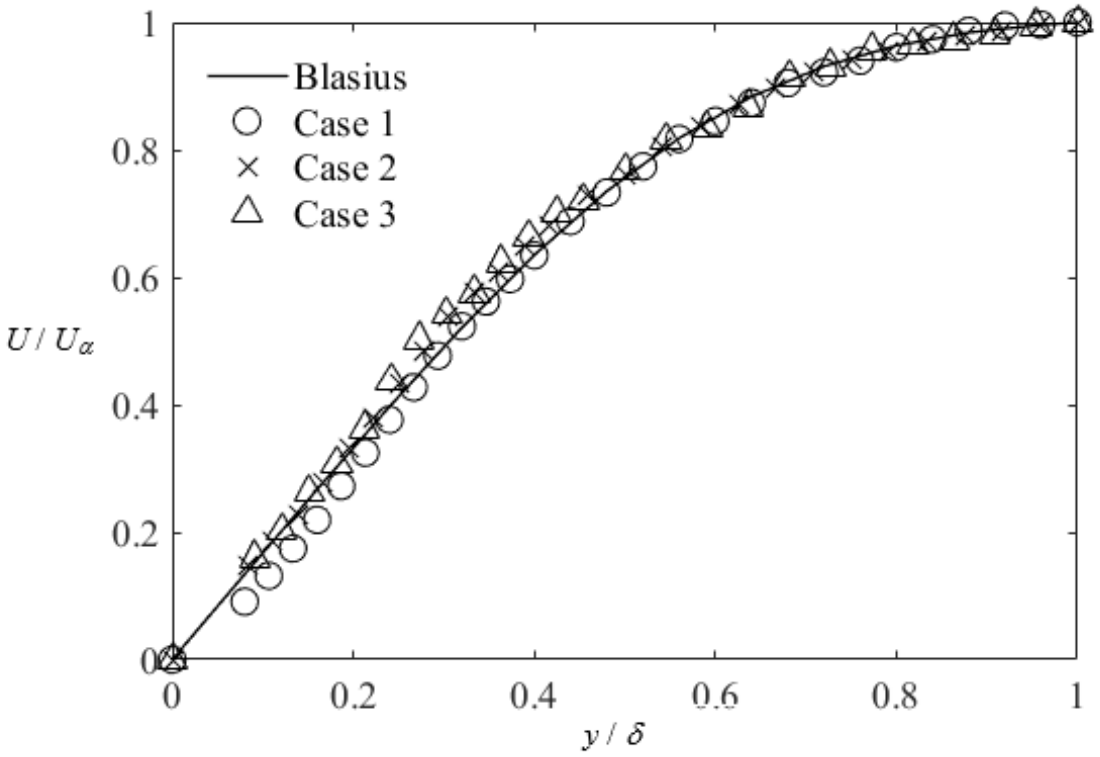

Fig. 3. Velocity profile, measured at x = 0.47 m

In this study, the thermochromic liquid crystals were utilized as a surface temperature indicator. Their color, detected at the thermocouple tip within a 100 pixels * 100 pixels window was directly calibrated with the temperature, measured by the thin leaf thermocouple. During the process, the temperature was gained from 26 to 30 °C with an increment of 0.2 °C. The signals were first recorded in RGB system and they were transformed to HSI, as suggestion of [12]. The signal of Hue, representing the color of liquid crystals and the signal of temperature was correlated using a 5^{th} order polynomial equation as illustrated in Fig. 4. In the figure, the uncertainty of the technique is provided as the error bar. The equation was yielded as follows:

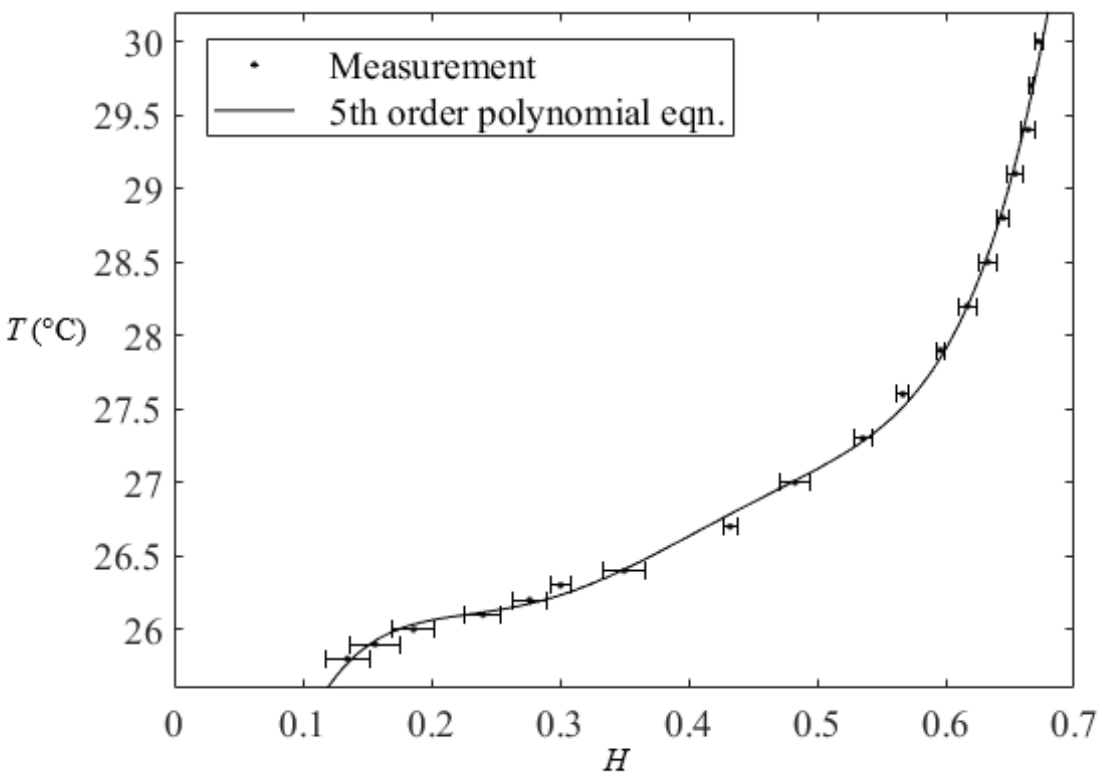

Fig. 4. Calibrated relation between the Hue signal and the surface temperature

$$T = 1,222.39H^5 - 2,247.90H^4 + 1,590.33H^3 - 531.81H^2 + 85.76H + 20.67 \quad (3)$$

where the goodness of fit is 0.998. In the current study, the heat transfer rate of 300 W was kept constant throughout the experiment. Thus, the local convective coefficient, h_x on the heating surface is given by:

$$h_x = Q / A(T_s - T_\alpha) \quad (4)$$

The local Nusselt number, Nu_x is given by [13] as:

$$Nu_x = h_x x / k \quad (5)$$

3 Results

When the flow visualization technique using thermochromic liquid crystals were employed, the thermal distribution of the flat surface under the conditions with and without the disturbance of low frequency ultrasonic waves are first recorded in RGB format as depicted in Fig. 5. In the figure, the mainstream flows from left to right with the velocity of 0.126 and the vertical strips are the thin leaf thermocouple. Following the increase in local Reynolds number, Fig. 5(a) shows that the color of liquid crystals changes from green to dark blue. However, when the ultrasonic waves were released at Re_x = 66,661,

the green color clearly emerges at the downstream of the heating surface. The size of this region enlarges following the wave frequency.

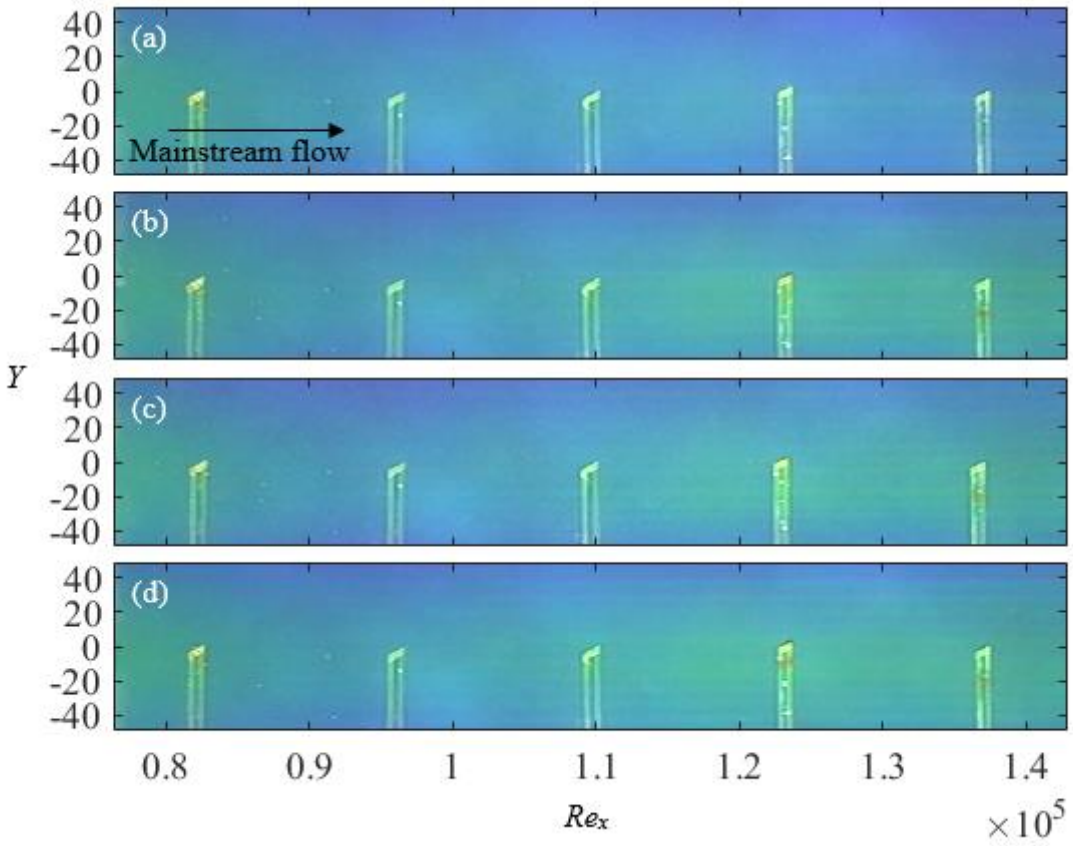

Fig. 5. RGB signal under the condition (a) without ultrasound, and with ultrasound having frequency of (b) 25, (c) 33, and (d) 40 kHz

After the RGB signal was transformed to the *H*, the contour of surface temperature was obtained via Eq. (3) and presented in Fig. 6. Because the liquid crystals on the metal surface of thermocouples reflected wrong color comparing with the surrounding region, this area was masked to present the location of thermocouples. Without the ultrasound, the parabolic profile of low temperature appears at the upstream of test area and the magnitude of temperature decreases in accordance with the streamwise distance. The surface temperature ranges between 27.5 and 29 °C as shown in Fig. 6(a). When the 25, 33, and 40 kHz ultrasonic waves was applied to the flow, they can decrease the surface temperature at the downstream to approximately 27.5°. The size of this region expands following the magnitude of wave frequency. However, it is noted that the temperature distribution at the upstream of test region doesn't change even though the transducer was installed at Re_x = 66,661.

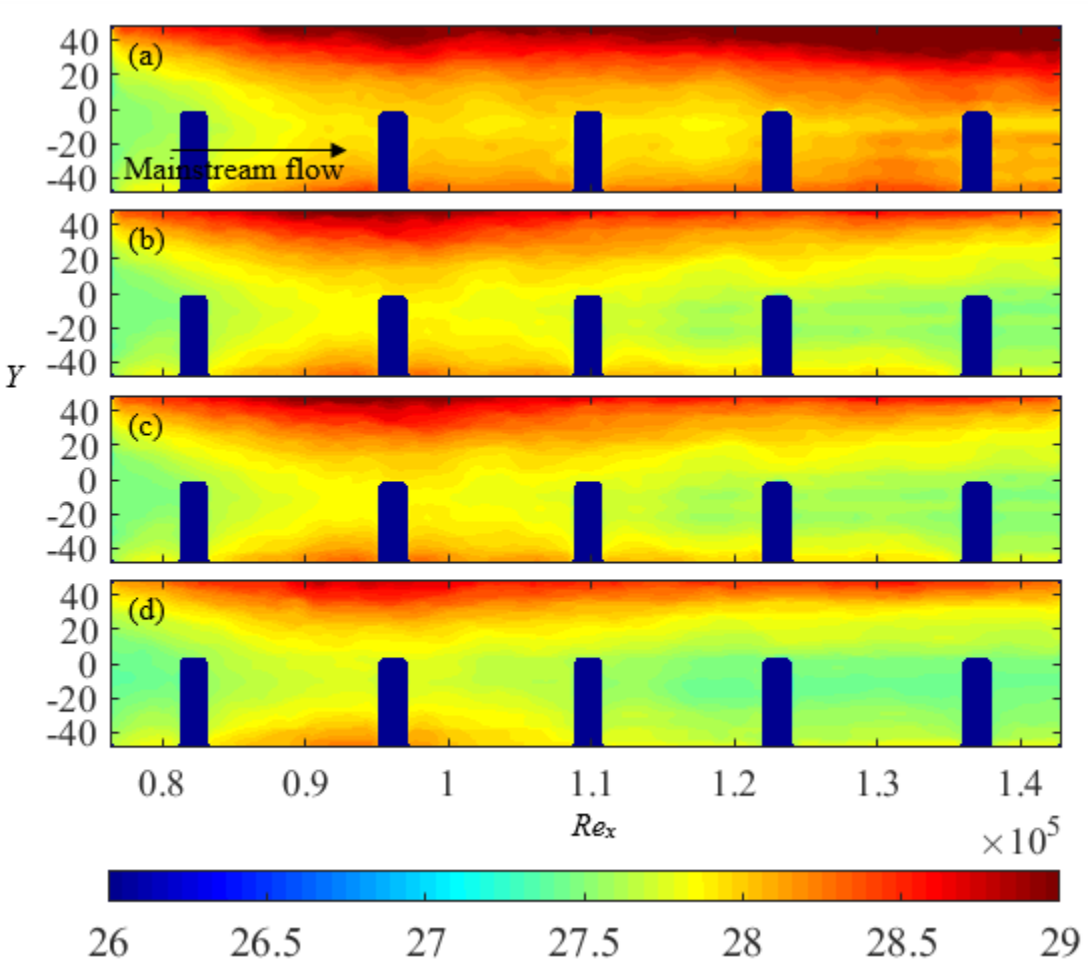

Fig. 6. Surface temperature (°C) under the condition (a) without ultrasound, and with ultrasound having frequency of (b) 25, (c) 33, and (d) 40 kHz

After the convective coefficient of the heating surface was determined via Eq. (4), the contour of Nusselt number was then achieved as depicted in Fig. 7. During the Re_x from 78,000 to 142,000, the Nu_x increases following the streamwise distance as those calculated using formula of [14]. The maximum Nu_x of approximately 560 appears the downstream of the test area. At Re_x = 142,000, this magnitude gains to approximately 630, 680, and 730 when the wave frequency is 25, 33, and 40 kHz, respectively. Moreover, the parabolic region of the high Nu_x on the heating plate is clearly observable under the influence of 25-40 kHz ultrasound. This is a strong evidence, showing that the ultrasonic waves can directly increase the heat transfer of the heating surface under the laminar shear layer.

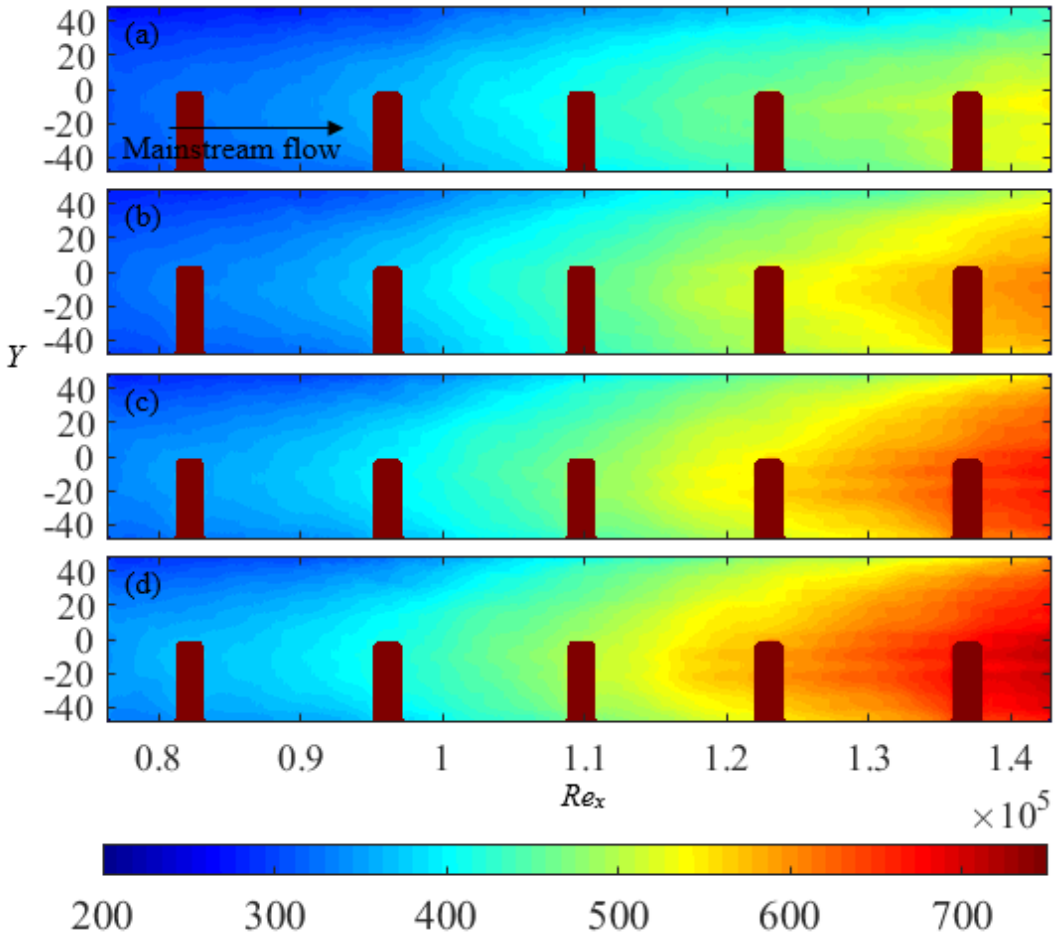

Fig. 7. Nusselt number contour under the condition (a) without ultrasound, and with ultrasound having frequency of (b) 25, (c) 33, and (d) 40 kHz

The contour of Nusselt number ratio on the heating surface under the condition with and without the ultrasound, Nu_w/Nu_0 is presented as illustrated in Fig. 8. Its magnitude is presented between 0.95 – 1.2 at the color bar below. From Fig. 8(a) or case 1, the Nusselt number under the 25 kHz ultrasonic waves was mostly higher than that at the condition without the ultrasonic waves or $Nu_w/Nu_0 > 1$ when the $Re_x > 100{,}000$. This could be considered as the incident region of ultrasonic waves. At the upstream of this point, the Nu_w/Nu_0 is approximately 1 in both streamwise and spanwise directions. The wave incident region appears like a wedge, which might be mutually induced by the generated bubbles on the test surface under the transducer as depicted in Fig. 9. However, the size of these bubbles is on the order of 2 μm. With the appearance of the bubbles, this confirms that the acoustic streaming is strengthen [10] and cause the overlap between the location of transducer and enhanced heat transfer. The maximum Nu_w/Nu_0 increases following the ultrasonic frequency, which is consistent with the suggestion of [15]. The maximum Nusselt number ratio is found at the core of each streak as approximately 14%, 17.5%, and 21.8% when the wave frequency is 25, 33, and 40 kHz, respectively. Furthermore, at the relatively higher wave frequency, the enhanced heat transfer region enlarges in both streamwise and spanwise directions.

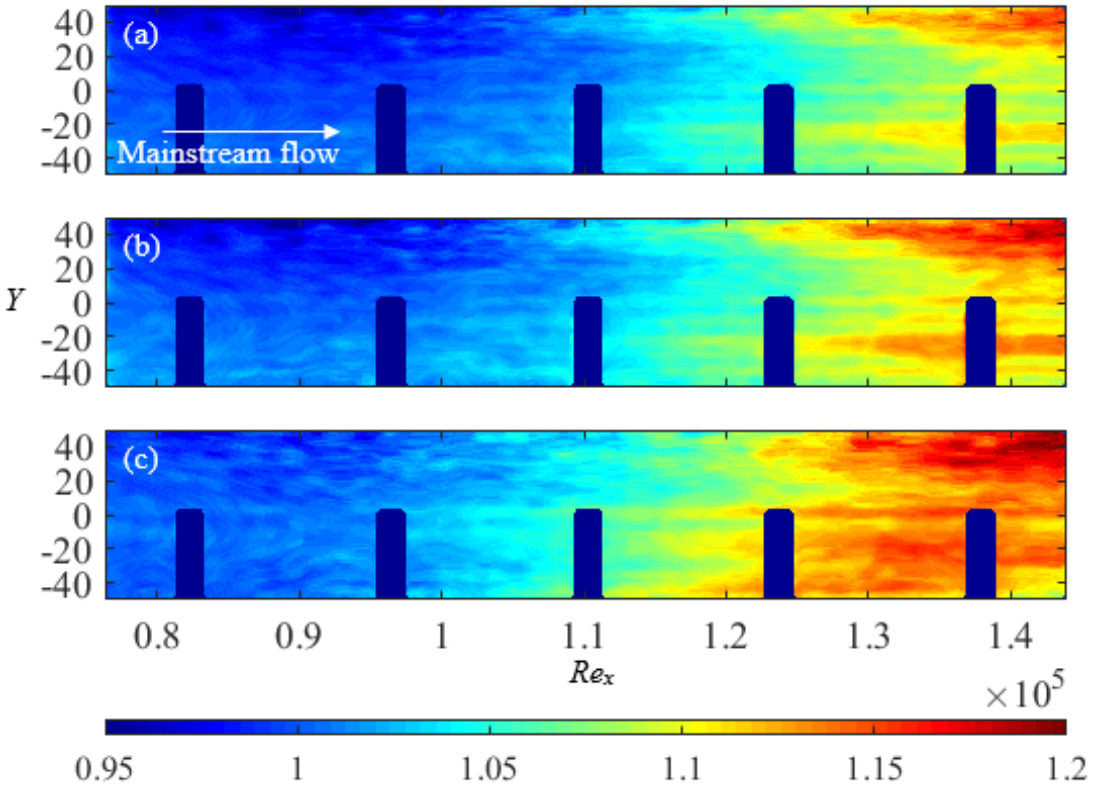

Fig. 8. Nusselt number ratio under case 1 at the wave frequency of (a) 25, (b) 33, and (c) 40 kHz

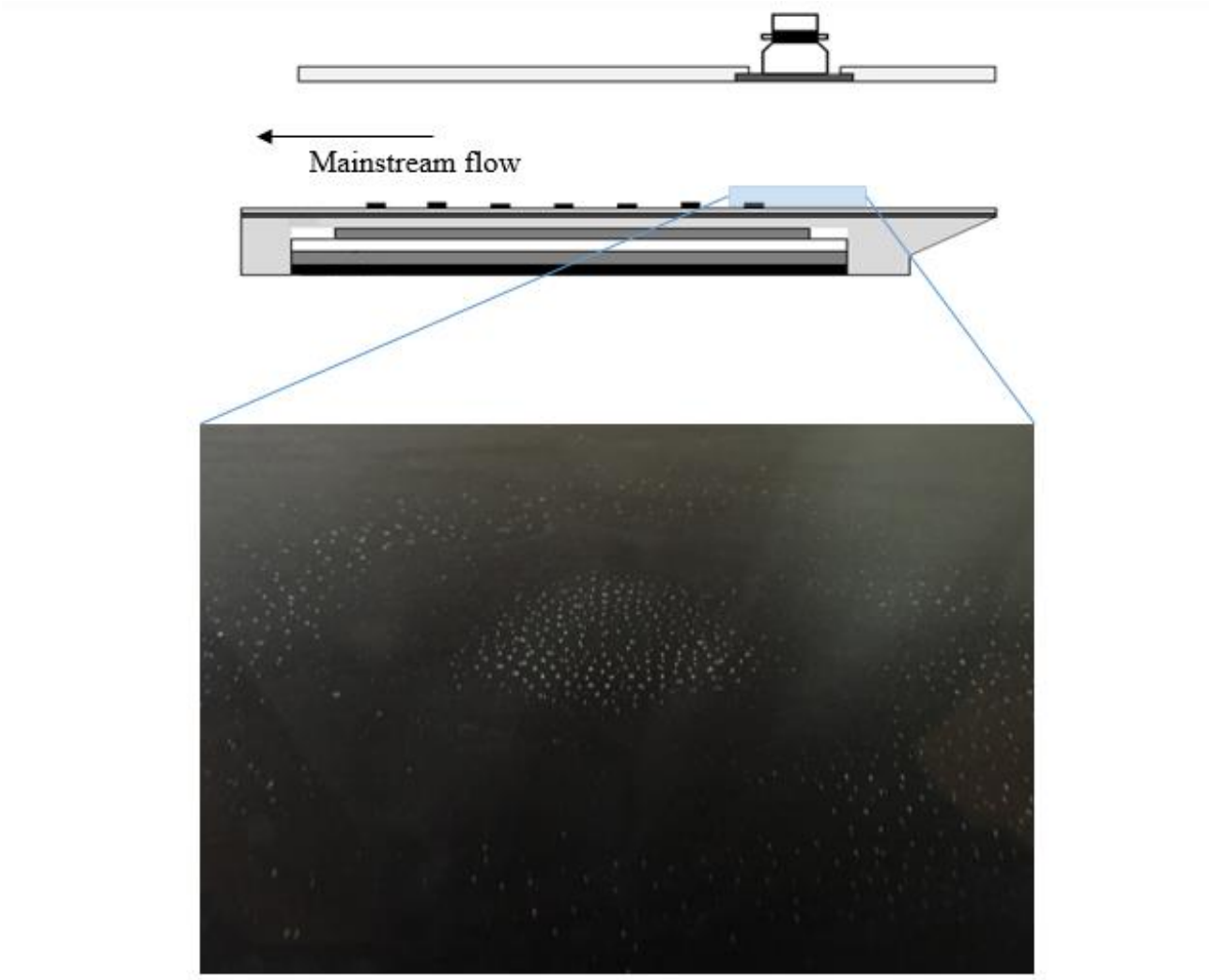

Fig. 9. Bubbles on the test plate under the transducer

In this study, the pattern of the bubbles on the test surface at the location of the ultrasonic transducer was also observed and it occurred differently as depicted in Fig. 10. The main effects of this change are wave frequency, time, and the mainstream velocity.

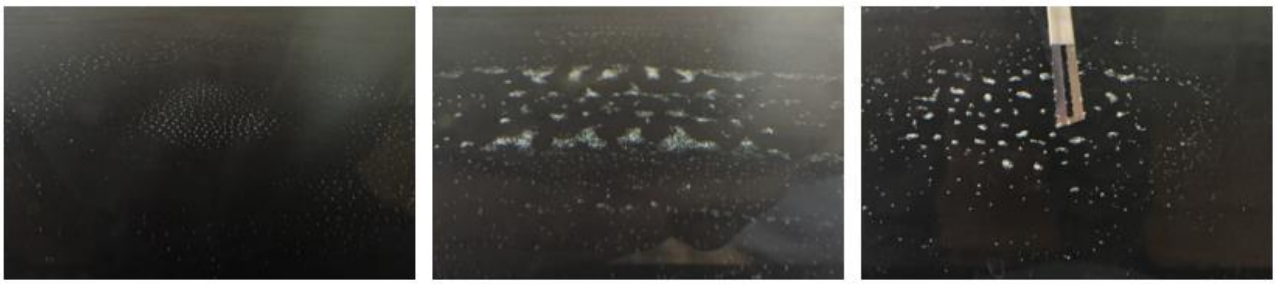

Fig. 10. The pattern of bubbles on the test surface at the location of the ultrasonic transducer

When the mainstream velocity increases in case 2, the pattern of Nusselt number also changes and the capability of heat transfer enhancement decreases, comparing with those yielded from case 1.

The region of wave incidence commences at the Re_x of approximately 130,000 when the transducer was installed at Re_x = 74,375 as shown in Fig. 11. The wedge structure is also observed at Re_x = 130,000 – 160,000 but the strength of the increasing heat transfer occurs like the region of Re_x = 100,000 – 120,000 in case 1. In this region, the averaging augmentation of heat transfer is approximately 5% above the laminar state.

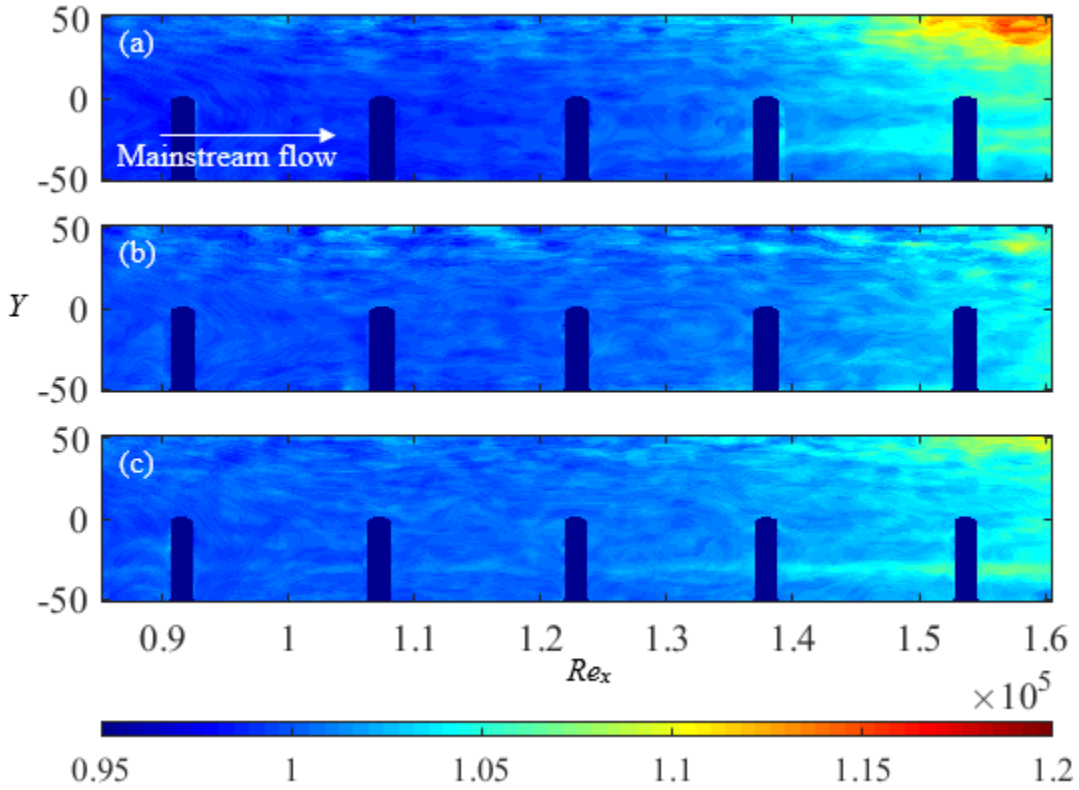

Fig. 11. Nusselt number ratio under case 2 at the wave frequency of (a) 25, (b) 33, and (c) 40 kHz

Finally, when the U_α was relatively maximized, the average Nusselt number ratio is approximately 1 through the entire surface, as depicted in Fig. 12. Unlike case 1 and 2, the region of highly enhanced heat transfer disappears. However, this region is supposed to be further downstream beyond this test area because the average Nu_w/Nu_0 is increasing along the streamwise direction. Furthermore, it is apparently noted that the upstream region in this contour has the Nu_w/Nu_0 below 1. This happens when the beam of ultrasonic waves is incident on the downstream region and retards the near wall flow. Consequently, it decrease the heat transfer capability at the upstream region under case 3.

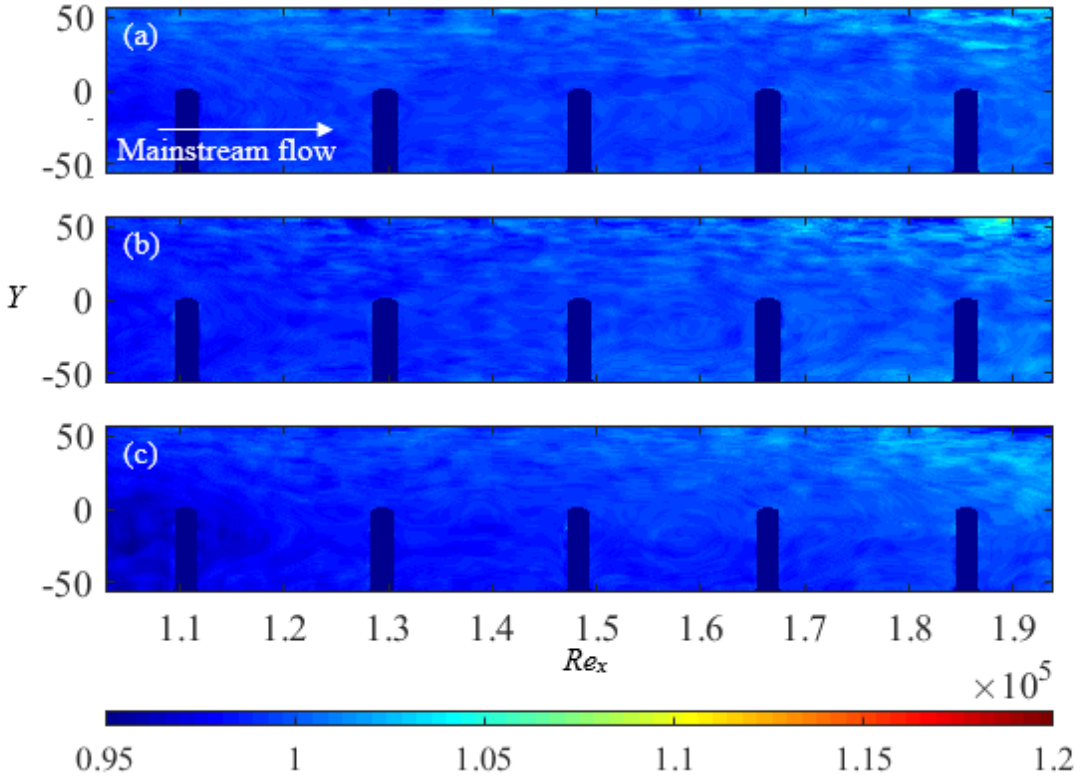

Fig. 12. Nusselt number ratio under case 3 at the wave frequency of (a) 25, (b) 33, and (c) 40 kHz

4 Conclusions

The results from this visualization showed that the ultrasound causes the acoustic cavitation or bubbles on the test surface at the location of the flat transducer. This led to the destabilization of the boundary layer and induced the heat transfer augmentation of the heating surface. The induced region occurred like wedge structure, caused by the upstream bubbles. The maximum Nusselt number appeared at the core of each wedge and was up to 14%, 17.5%, and 21.8% at the wave frequency of 25, 33, and 40 kHz, respectively. This region moved further downstream following the increase in Reynolds number and these results clearly presented that the heating surface was affected by the transducer directly. Therefore, these obtained results clarified the process of heat transfer enhancement using the low frequency ultrasonic waves.

Acknowledgement

The authors gratefully acknowledge the financial support for project R-M 6.59 from the Kasetsart University Research and Development Institute (KURDI). Also, we sincerely thank for the valuable suggestions from Prof. Dr. Tanongkiat Kiatsiriroat and Assoc. Prof. Dr. Chawalit Kittichaikarn.

References

[1] Legay M, Gondrexon N, Le Person S, Boldo P and Bontemps A. Enhancement of heat transfer by ultrasound: review and recent advances. *Int. J. Chem. Eng.,* Vol. 2011, pp 1-17, 2011.

[2] Webster E. Cavitation. *Ultrasonics,* Vol. 1, No. 1, pp 39-48, 1963.

[3] Neppiras EA. Acoustic cavitation series: part one: Acoustic cavitation: an introduction. *Ultrasonics*, Vol. 22, No. 1, pp 25-28, 1984.

[4] Lighthill J. Acoustic streaming. *J. Sound Vib.,* Vol. 61, No. 3, pp 391–418, 1978.

[5] Fand RM and Kave J. Acoustic streaming near a heated cylinder. *J. Acoust. Soc. Am.,* Vol. 32, No. 5, pp 579–584, 1960.

[6] Monnot A, Boldo P, Gondrexon N and Bontemps A. Enhancement of cooling rate by means of high frequency ultrasound. *Heat Transfer Eng.,* Vol. 28, No. 1, pp 3-8, 2007.

[7] Gondrexona N, Rousseleta Y, Legaya M, Boldo P, Le Personc S and Bontemps A. Intensification of heat transfer process: Improvement of shell-and-tube heat exchanger performances by means of ultrasound. *Chem. Eng. Process.*, Vol. 49, pp 936-942, 2010.

[8] Zhou D, Hu X and Liu D. Local convective heat transfer from a horizontal tube in an acoustic cavitation field. *J. Therm. Sci.,* Vol. 13, No. 4. pp 338-343, 2004.

[9] Inworn N and Chaiworapuek W. On the Thermal Characteristic of a Heating Flat Surface under Low Frequency Ultrasonic Waves. *Int. J. Heat Mass Transfer,* Vol. 122, pp 1153-1161, 2018.

[10] Sakamoto S and Watanabe Y. Effects of existence of microbubbles for increase of acoustic streaming. *Jpn. J. Appl. Phys.*, Vol. 38, pp 3050-3052, 1999.

[11] Barthes M, Mazue G, Bonnet D, Viennet R, Hihn JY and Bailly Y. Characterization of the activity of ultrasound emitted in a perpendicular liquid flow using Particle Image Velocimetry (PIV) and electrochemical mass transfer measurements. *Ultrasonics*, Vol. 59 pp 72-78, 2015.

[12] Russ JC. *The image processing handbook.* CRC Press, 2002.

[13] Çengel YA and Ghajar AJ. *Heat and mass transfer – fundamentals & applications.* McGraw-Hill, 2015.

[14] Kays WM and Crawford ME. *Convective heat and mass transfer*. McGraw-Hill, 1993.

[15] Vainshtein P, Fichman M and Gutfinger C. Acoustic enhancement of heat transfer between two parallel plates. *Int. J. Heat Mass Transfer,* Vol. 38, No. 10, pp 1893-1899, 1995.

Copyright Statement